Geochemical Perspectives Letters

On the oxidation state of arc magmas

Y. Moussallam[1,2*], G. Georgeais[1], S. Ding[1,3], J.-L. Devidal[4], B. Scaillet[5], C. Oppenheimer[6], A. Burgisser[7], E.F. Rose-Koga[5], K.T. Koga[5], N. Peters[8], A. Peccia[1], P. Samaniego[4], N. Métrich[9], P. Robidoux[10,11,12], M. Kawaguchi[13]

OPEN ACCESS

https://doi.org/10.7185/geochemlet.2611

Abstract

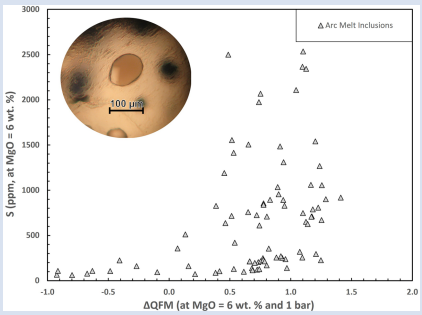

Arc magmas have long been considered significantly more oxidised than their ocean island and mid-ocean ridge counterparts, a characteristic widely attributed to infusion of the mantle wedge by fluids from subducted lithologies. However, here we show that at comparable degree of differentiation and sulfur content, arc magmas have comparable oxidation state to ocean island magmas. Our study is based on measurements of $Fe^{3+}/\Sigma Fe$ along with major and volatile elements in olivine and plagioclase hosted melt inclusions and matrix glasses from eleven volcanic systems located in arc settings worldwide. Accounting for fractional crystallisation (to MgO = 6 wt. %) we find that all systems lie on a reducing trend accompanying sulfur degassing, from QFM +0.9 (±0.2, 1σ) when S > 2000 ppm to QFM −0.2 (±0.6, 1σ) when S < 100 ppm (where QFM stands for the Quartz-Fayalite-Magnetite buffer). These findings reconcile the observed discrepancy between the oxidation states of xenoliths in arc magmas and gas emissions from arc volcanoes. We further show that fractional crystallisation influences the redox evolution of arc magmas to a comparable extent as, and sometimes counteracting, sulfur degassing.

Received 17 July 2025 | Accepted 5 March 2026 | Published 10 April 2026

Introduction

Constraining the oxidation state of arc magmas has long been of interest to petrologists and geochemists because the initial oxidation state of a melt plays a critical role in the sequence of phases that crystallise from it (*e.g.*, Osborn, 1959). Determining the oxidation state of the mantle source of these melts is in turn of interest for understanding the cycling of multiple valence state elements between the Earth's interior and exterior *via* subduction zones. Three main sample types have been used to constrain the oxidation state of arc magmas: (i) erupted lavas and tephra (*e.g.*, Carmichael, 1991), (ii) xenoliths carried in arc magmas (*e.g.*, Parkinson and Arculus, 1999), and (iii) crystal hosted melt inclusions (*e.g.*, Kelley and Cottrell, 2012).

However, while measurements of erupted products and xenoliths have been made for arc magmas around the world (*e.g.*, Hu *et al.*, 2024), measurements of crystal hosted melt inclusions (MIs) for arc lavas almost exclusively derive from a single site, the Mariana Arc (Brounce *et al.*, 2014; Kelley and Cottrell, 2009, 2012). One reason for the paucity of data of the latter type, in addition to challenging sample preparation, is that X-ray absorption near-edge structure (XANES) measurements of the valence state of Fe and S in water-rich silicate glasses are often compromised by beam damage (*e.g.*, Cottrell *et al.*, 2009, 2018; Shorttle *et al.*, 2015; Moussallam *et al.*, 2014, 2016, 2019, 2023). Yet these are the only measurements that directly measure the oxidation state of Fe and S (the most important multiple valence state elements) in the melt as opposed to reliance on proxies. Here we report $Fe^{3+}/\Sigma Fe$ measurements in melt inclusions from eleven arc volcanoes obtained by XANES spectroscopy at the iron K-edge, together with their volatile and major element concentrations.

1. Lamont-Doherty Earth Observatory, Columbia University, New York, USA
2. American Museum of Natural History, Department of Earth and Planetary Sciences, NY 10024, New York, USA
3. Department of Geological Sciences, University of Florida, Gainesville, FL, USA
4. Université Clermont Auvergne, CNRS, IRD, OPGC, Laboratoire Magmas et Volcans, F-63000 Clermont-Ferrand, France
5. ISTO, UMR 7327, Université d'Orléans-CNRS-BRGM, 1A rue de la Férollerie, 45071 Orléans cedex 2, France
6. Department of Geography, University of Cambridge, Downing Place, Cambridge, CB2 3EN, UK
7. Univ. Grenoble Alpes, Univ. Savoie Mont Blanc, CNRS, IRD, Univ. Gustave Eiffel, ISTerre, Grenoble, France
8. Department of Electronic and Electrical Engineering, University College London, UK
9. Université Paris Cité, Institut de Physique du Globe de Paris, CNRS, 75005 Paris, France
10. Universidad Andres Bello, Facultad de Ingenieria, Antonio Varas 880, Santiago, Chile
11. Millennium Institute on Volcanic Risk Research - Ckelar Volcanoes, Avenida Angamos 0610, Antofagasta, Chile
12. Consortium de Recherche en Exploration Minérale (CONSOREM), Département des Sciences Appliquées, Université du Québec à Chicoutimi, 555 Boul. de l'Université, Chicoutimi, Québec G7H 2B1, Canada
13. Earthquake Research Institute, University of Tokyo, Japan

* Corresponding author (email: yves.moussallam@ldeo.columbia.edu)

Samples and Methods

Sample sites were chosen because of the relatively mafic composition of their magmas (Fig. 1). They include Yasur, Aoba/Ambae, and Ambrym in Vanuatu, Shinmoedake and Aso in Japan, Okmok in Alaska, Fuego in Guatemala, San Cristóbal in Nicaragua, Cotopaxi in Ecuador, Villarrica in Chile, and Stromboli in Italy. Detailed sample description and processing is provided in the Supplementary Information, together with details of the Fourier Transform Infrared Spectroscopy and electron probe microanalyses.

XANES analyses. We performed Fe K-edge XANES spectroscopy at beamline I18 at the Diamond Light Source (DLS), UK. X-rays were focused with Kirkpatrick-Baez mirrors to a beam size of 5 μm (horizontal) × 5 μm (vertical). The beamline uses a liquid nitrogen cooled double crystal monochromator with silicon crystals and the Si (333) reflection was used to maximise the energy resolution. The measurements were performed in fluorescence mode. We used an energy dispersive Vortex ME-4 silicon drift detector positioned at 90° to the incident beam. The sample was positioned so that the normal to the sample surface was at 45° to the incident X-ray beam. Standard analytical conditions for XANES at I18 yield a photon flux of 10^{10} photon/s by attenuating (using a combination of aluminium foils and a slit) a 10^{12} photon/s primary beam upstream of the ion chamber. The beam can then be further attenuated (using Al foil).

We performed a series of tests to tune analytical conditions so as to avoid beam damage in our samples. We used:

1. A natural melt inclusion from Stromboli volcano (SHE750_cr1) containing 1.9 wt. % H_2O.
2. A natural melt inclusion from Okmok volcano (54D-MIol3) containing 2.0 wt. % H_2O.
3. A natural melt inclusion from Shinmoedake volcano (Shinm_cr23_mi) containing 2.2 wt. % H_2O.
4. A synthetic hydrated experimental glass of Villarrica 2015 composition (VillaS5_new_b) containing 4.5 wt. % H_2O.
5. A natural melt inclusion from Fuego volcano (F2018_cr12_mi) containing 6.2 wt. % H_2O.

We positioned the monochromator at a fixed energy of 7114 eV, corresponding to the oxidised peak of the pre-edge region. We then opened the shutter and counted the fluoresced X-rays every second for 660 to 1000 s (approx. 10 to 17 min) (Fig. 2). Tests were performed attenuating the beam with either 100 μm or 250 μm Al plates, resulting in attenuation to about 16 % and 1 % of the original flux respectively (equivalent to ~10^9 and ~10^8 photon/s respectively or ~10^8 and 10^7 photon/s/μm^2 respectively) (Moussallam *et al.*, 2019). We found that with 250 μm Al plates, henceforth referred to as the "high attenuation" setup, even a glass containing 6.2 wt. % H_2O could be analysed without beam damage under our analytical conditions. These conditions are similar to those of Moussallam *et al.* (2019) who showed that at the same beamline under the same analytical conditions no beam damage was occurring when analysing a glass with 5.2 wt. % H_2O. We found that with a 100 μm Al plate, conditions similar to those used by Moussallam *et al.* (2016, 2023), henceforth referred to as the "moderate attenuation" setup, glasses with up to 2.2 wt. % H_2O could be analysed without beam damage under our analytical conditions. All MIs containing more than 2.2 wt. % H_2O were therefore analysed using the high attenuation setup while the other melt inclusions, and all matrix glasses were analysed using the moderate attenuation setup. Because the high attenuation setup leads to fewer fluorescent photon counts and hence lower quality spectra, dwell time at each energy step was increased (energy step sizes and dwell times given in Table S-1) and three to four scans were acquired *per* melt inclusion and co-added. Spectra showing any structure in the edge and post-edge region were rejected (see Fig. S-6 in Moussallam *et al.*, 2014, for an example of contaminated spectra).

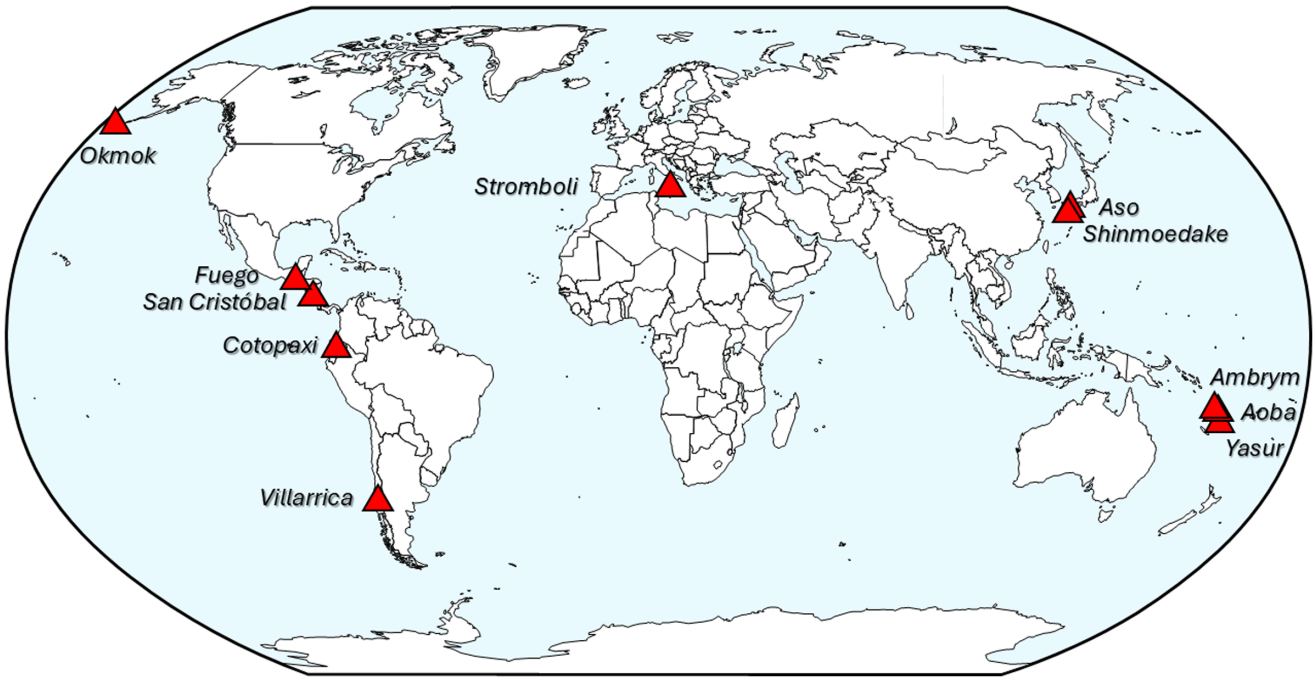

Figure 1 World map showing the locations of arc volcanoes investigated in this study, namely Yasur, Aoba/Ambae, Ambrym, Shinmoedake, Aso, Fuego, San Cristóbal, Cotopaxi, Villarrica, Okmok and Stromboli.

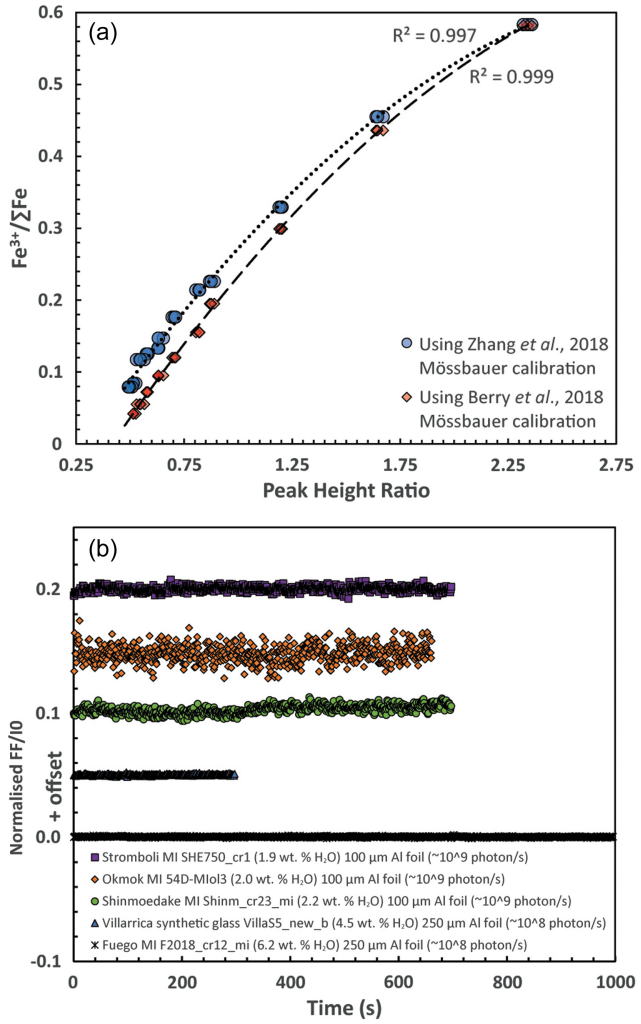

Figure 2 **(a)** Calibration line of the peak height ratio determined by XANES compared with $Fe^{3+}/\sum Fe$ ratios determined by Mössbauer spectroscopy in basaltic standard glasses from the Smithsonian NMNH (Mössbauer $Fe^{3+}/\sum Fe$ values from Zhang *et al.*, 2018 and Berry *et al.*, 2018 are shown). **(b)** Time series of normalised fluoresced intensity (FF) over I0 at 7114 eV integrated over 1 s intervals the five natural melt inclusions and synthetic glasses used for beam damage assessment. The Villarrica, Shinmoedake, Okmok and Stromboli glasses FF/I0 are offset by 0.05, 0.1, 0.15 and 0.2, respectively, for visibility. The variation in scatter between measurements is a function of the detector position which was adjusted between each sample.

The pre-edge region (7110–7118 eV) was fitted using a combination of a linear function and a damped harmonic oscillator function to fit the baseline and fitted by a combination of two gaussian functions. The relative intensity at the ~7112.2 eV and ~7114.0 eV peaks was then used to calibrate the spectra to the published $Fe^{3+}/\sum Fe$ ratios of the NMNH 117393 basalt reference glasses (Cottrell *et al.*, 2009) provided by the Smithsonian Institution National Museum of Natural History and using both the $Fe^{3+}/\sum Fe$ values reported in Zhang *et al.* (2018) and Berry *et al.* (2018) (Fig. 2). Repeat measurements ($n = 39$) on the twelve standards (all analysed using moderate attenuation) yielded a standard deviation of ±0.003 on the measured $Fe^{3+}/\sum Fe$ ratios (relative error) which translate to a standard deviation of ±0.04 on the calculated fO_2. Standard deviation using the high attenuation setup with two co-added spectra was determined as ±0.012 by Moussallam *et al.* (2019) (which translates to a standard deviation of ±0.14 on the calculated fO_2). We report this error here but note that in the present study we co-added three to four spectra each time so the error should be smaller. The absolute error is linked to the interpretation of the NMNH 117393 basalt reference glasses Mössbauer spectra and we show the calibrations resulting from both interpretations (Zhang *et al.*, 2018; Berry *et al.*, 2018) here.

Reverse fractional crystallisation calculation. To assess the effect of pre-entrapment crystallisation on $Fe^{3+}/\sum Fe$ (*e.g.*, Sun and Lee, 2022), we modelled reverse crystallisation paths for our melt inclusions using Petrolog3 (Danyushevsky and Plechov, 2011). We used the model of Ford *et al.* (1983) for olivine, the model of Ariskin *et al.* (1993) for plagioclase and the model of Ariskin *et al.* (1988) for clinopyroxene. This combination was used as it yielded reverse fractional crystallisation paths that most closely reproduced the trend in CaO *vs.* MgO observed in the natural melt inclusions and matrix glasses data (Fig. S-4). Note that these models assume a fully incompatible behaviour for Fe^{3+} in the olivine, clinopyroxene and plagioclase phases. Reverse fractional crystallisation calculations, which yield restored values of $Fe^{3+}/\sum Fe$, volatile contents, and major element compositions, were performed until the melt reached a value of 6 wt. % MgO, the highest value recorded in the data set (Fig. S-4). An alternative, empirical, modelling approach is presented in the SI. Post-entrapment crystallisation (PEC) for olivine hosted inclusions was calculated using Petrolog3 assuming a closed system for oxygen. The resulting PEC estimates range from −21 to +3 %, with an average of −2 % and standard deviation of ±3 %. Given these results we did not modify the MI compositions from their measured values.

Results and Discussion

We determined the $Fe^{3+}/\sum Fe$ ratio of 81 melt inclusions and 70 matrix glasses using XANES. The raw data for melt inclusions and matrix glasses are presented in Tables S-2 to S-6. We found that matrix glasses, clear of any visible alteration, exhibited a wide range of $Fe^{3+}/\sum Fe$ ratios, even within single samples. For instance, for Okmok glasses, $Fe^{3+}/\sum Fe$ ratios ranged from 0.19 to 0.54 (Tables S-5 and S-6). Most matrix glasses were significantly more oxidised than melt inclusions, with extreme values reaching up to QFM +5, uncorrelated with major or volatile element composition and with large variations in oxidation state recorded between areas of glass fragments located only a few millimetres apart. Based on these observations we consider that a significant proportion of our matrix glass $Fe^{3+}/\sum Fe$ measurements are unlikely to be representative of the original melt, and we consider that they reflect variable degrees of oxidation due to partial re-equilibration with erupted gas and/or the atmosphere during eruption. Consequently, we did not consider matrix glasses further in this study.

Raw melt inclusion $Fe^{3+}/\sum Fe$ ratios show no correlation with major or volatile (Fig. 3a) element compositions, with all r^2 values below 0.4. However, the analysed melt inclusions span a wide compositional range ($46.8 < SiO_2 < 62.8$ wt. %; Table S-3), partly reflecting variable degrees of differentiation. To account for this effect and compare melt inclusions at a common differentiation stage, we modelled reverse crystallisation paths using Petrolog3 (Danyushevsky and Plechov, 2011), back to MgO = 6 wt. % (results reported in Table S-7). After this restoration, a trend emerges between the oxidation state of melt inclusions and their S content (Fig. 3b,c). Melt inclusions with higher S contents are consistently more oxidised than those with lower S contents. On average, melt inclusions with S > 2000 ppm have an oxidation state of QFM +1.0 (±0.2, 1σ; $n = 6$), while those with S < 100 ppm have an oxidation state of QFM −0.2 (±0.6, 1σ; $n = 7$). Melt fO_2 is calculated from

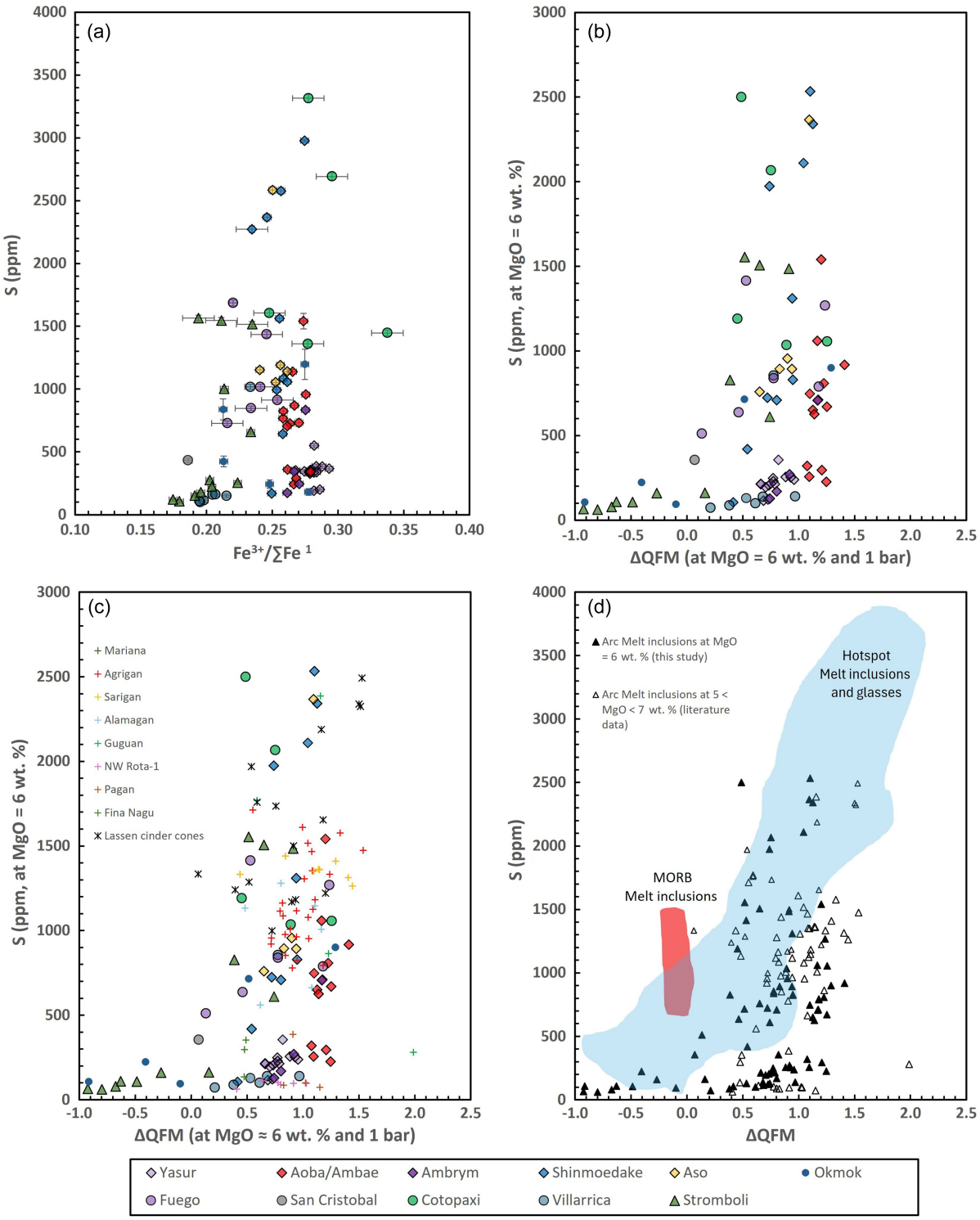

Figure 3 **(a)** Sulfur content *versus* oxidation state of melt inclusions plotted as $Fe^{3+}/\sum Fe$ calculated using the Mössbauer $Fe^{3+}/\sum Fe$ values from Zhang *et al.* (2018). Error bars show 1σ. **(b)** Sulfur content *versus* oxidation state (plotted as deviation from the QFM buffer using the equation of Kress and Carmichael, 1991) of melt inclusions after reversing fractional crystallisation to a common value of MgO = 6 wt. %. **(c)** Same as **(b)** with the addition of melt inclusions (and pillow glasses) data from the Marianna arc (Kelley and Cottrell, 2012; Brounce *et al.*, 2014, 2016) and Lassen cinder cones (Muth and Wallace, 2021), all with MgO contents between 5 and 7 wt. %. **(d)** Comparison between the sulfur content *versus* oxidation state fields recorded by melt inclusions, embayments and matrix glasses from arc volcanoes (same data set as in **(c)**), hotspot volcanoes (from Fig. 7 in Moussallam *et al.*, 2019) and mid-ocean ridge volcanoes (data set of Moussallam *et al.*, 2023) from the Southwest Indian Ridge). Note that Hotspot melt inclusions and glasses in the database used to draw the field are on average at MgO = 6.1 ± 1.0 wt. % while MORB Melt inclusions are on average at MgO = 6.4 ± 1.3 wt. % (1σ).

$Fe^{3+}/\sum Fe$ using Equation (7) from Kress and Carmichael (1991) at 1 bar and using the Petrolog3 calculated equilibrium temperature; QFM refers to the Quartz-Magnetite-Fayalite mineral redox buffer as reported in Frost (1991).

We can compare these results with other studies that have determined the oxidation state of melt inclusions (and pillow glasses) in arc magmas by XANES spectroscopy at the Fe K-edge. These include studies in the Mariana arc (Kelley and Cottrell, 2012; Brounce *et al.*, 2014, 2016) and a study of cinder cones in the Lassen region (California, USA) (Muth and Wallace, 2021). For the comparison with our data, corrected to MgO = 6 wt. %, to be meaningful, we only report in Figure 3c literature data from Mariannas and Lassen with MgO contents between 5 and 7 wt. % (*i.e.* directly comparable to our MgO = 6 wt. % data). The distributions of our new data points and existing ones coincide and overlap, mostly falling within the same range in oxidation state at a given S content. The observed trend between the sulfur content of melt inclusions and their oxidation state is strengthened by the addition of literature data extending the trend to slightly higher oxidation states. It therefore appears that, as previously demonstrated for hotspot volcanoes (Moussallam *et al.*, 2014, 2016, 2019; Brounce *et al.*, 2017), sulfur degassing in arc volcanoes is accompanied by a reduction of the melt oxidation state. In the SI we explore how available gas-melt equilibrium degassing models compare to the observed trend.

We note that our observations reconcile an apparent discrepancy in the literature regarding the oxidation states of arc magmas. Most estimates of the oxygen fugacities of the sub-arc mantle, from mineral oxybarometry in xenoliths and lavas (*e.g.*, Cottrell *et al.*, 2021 and references therein) or trace element systematics in arc lavas (*e.g.*, Zhao *et al.*, 2022) cluster around QFM +1, while those from the 'restoration' of volcanic gases of arc volcanoes to magmatic temperatures cluster around QFM (Moussallam *et al.*, 2024). The one log unit difference in oxidation state can be readily explained by degassing (Fig. 3).

Another interesting result is that, at similar degrees of differentiation (MgO ≈ 6 wt. %) and sulfur contents (~2500 ppm), arc magmas are not more oxidised than their hotspot counterparts. Hotspot magmas record oxidation states around QFM +1.2 under these conditions and even more oxidised conditions at higher sulfur contents, taken as evidence of recycled oxidised crustal material brought out of the deep earth by mantle plumes (Moussallam *et al.*, 2019) (Fig. 3d). In fact, there is a significant overlap between the arc and hotspot data sets (Fig. 3d). However, the reducing trend with sulfur degassing differs between hotspot and arc magmas, showing a constant slope for hotspot magmas and a hockey stick trend for arc magmas. This difference is likely due to the significant variation in water content between the two magma types. In contrast, the oxidation state of melt inclusions in mid-ocean ridge magmas shows no change in oxidation state with sulfur content (*e.g.*, Moussallam *et al.*, 2023) (Fig. 3d). The sulfur content of MORB is thought to be primarily controlled by equilibrium with sulfide (*e.g.*, Mathez, 1976), such that sulfur degassing in MORBs is an uncommon, yet documented, process (*e.g.*, Shorttle *et al.*, 2015).

Conclusions

We have analysed the oxidation states of arc magmas from eleven volcanic systems by measuring $Fe^{3+}/\sum Fe$ ratios along with major and volatile elements in olivine and plagioclase hosted melt inclusions. Once corrected for the effect of fractional crystallisation, we found that arc magmas define a trend of decreasing oxidation state with decreasing sulfur content. Thus, both degassing and differentiation can influence redox conditions of arc magmas to a comparable magnitude yet potentially in opposing directions (reducing and oxidising, respectively). When compared at similar degrees of differentiation and sulfur contents, the oxidation states of arc magmas can be similar to those of hotspot volcanoes.

Acknowledgements

Analytical work was carried out at Diamond Light Source using beamline I18 (proposal number SP36021-1) with invaluable support from Susan Nehzati and Konstantin Ignatyev. EFR-K thank Dr Akira Yoshiasa, and Dr. Toshiaki Hasenaka for their help on the field during the 2020 sampling campaign in Japan. We are very grateful to Marco Pistolesi for providing samples from Stromboli. We are grateful to Ery Hughes and two anonymous reviewers for providing valuable comments improving the quality of the manuscript.

Editor: Helen Williams

Open Research

Raw X-ray absorption near-edge structure spectra at the iron K-edge are archived on https://figshare.com/ [Moussallam, Y. (2025) ARC XANES SPECTRA RAW. *figshare*, dataset. https://doi.org/10.6084/m9.figshare.29509223.v1]. Raw FTIR data and PyIRoGlass outputs are archived on https://figshare.com/ [Moussallam, Y. (2025) ARC FTIR Spectra and Fit. *figshare*, dataset. https://doi.org/10.6084/m9.figshare.30657611.v1].

Additional Information

Supplementary Information accompanies this letter at https://www.geochemicalperspectivesletters.org/article2611.

Cite this letter as: Moussallam, Y., Georgeais, G., Ding, S., Devidal, J.-L., Scaillet, B., Oppenheimer, C., Burgisser, A., Rose-Koga, E.F., Koga, K.T., Peters, N., Peccia, A., Samaniego, P., Métrich, N., Robidoux, P., Kawaguchi, M. (2026) On the oxidation state of arc magmas. *Geochem. Persp. Let.* 39, 42–47. https://doi.org/10.7185/geochemlet.2611

References

Ariskin, A.A., Barmina, G.S., Frenkel, M.Y., Yaroshevskiy, A.A. (1988) Simulating low-pressure tholeiite-magma crystallization. *Geochemistry International* 25, 21–37.

Ariskin, A.A., Frenkel, M.Ya., Barmina, G.S., Nielsen, R.L. (1993) Comagmat: a Fortran program to model magma differentiation processes. *Computers & Geosciences* 19, 1155–1170. https://doi.org/10.1016/0098-3004(93)90020-6

Berry, A.J., Stewart, G.A., O'Neill, H.St.C., Mallmann, G., Mosselmans, J.F.W. (2018) A re-assessment of the oxidation state of iron in MORB glasses. *Earth and Planetary Science Letters* 483, 114–123. https://doi.org/10.1016/j.epsl.2017.11.032

Brounce, M.N., Kelley, K.A., Cottrell, E. (2014) Variations in $Fe^{3+}/\Sigma Fe$ of Mariana Arc Basalts and Mantle Wedge fO_2. *Journal of Petrology* 55, 2513–2536. https://doi.org/10.1093/petrology/egu065

Brounce, M., Kelley, K.A., Stern, R., Martinez, F., Cottrell, E. (2016) The Fina Nagu volcanic complex: Unusual submarine arc volcanism in the rapidly deforming southern Mariana margin. *Geochemistry, Geophysics, Geosystems* 17, 4078–4091. https://doi.org/10.1002/2016GC006457

Brounce, M., Stolper, E., Eiler, J. (2017) Redox variations in Mauna Kea lavas, the oxygen fugacity of the Hawaiian plume, and the role of volcanic gases in Earth's oxygenation. *Proceedings of the National Academy of Sciences* 114, 8997–9002. https://doi.org/10.1073/pnas.1619527114

Carmichael, I.S.E. (1991) The redox states of basic and silicic magmas: a reflection of their source regions? *Contributions to Mineralogy and Petrology* 106, 129–141. https://doi.org/10.1007/BF00306429

Cottrell, E., Kelley, K.A., Lanzirotti, A., Fischer, R.A. (2009) High-precision determination of iron oxidation state in silicate glasses using XANES. *Chemical Geology* 268, 167–179. https://doi.org/10.1016/j.chemgeo.2009.08.008

Cottrell, E., Lanzirotti, A., Mysen, B., Birner, S., Kelley, K.A., Botcharnikov, R., Davis, F.A., Newville, M. (2018) A Mössbauer-based XANES calibration for hydrous basalt glasses reveals radiation-induced oxidation of Fe. *American Mineralogist* 103, 489–501. https://doi.org/10.2138/am-2018-6268

Cottrell, E., Birner, S., Brounce, M., Davis, F., Waters, L., Kelley, K. (2021) Oxygen fugacity across tectonic settings. In: Moretti, R., Neuville, D.R. (Eds.) *Magma Redox Geochemistry*. American Geophysical Union, Hoboken, 33–61. https://doi.org/10.1002/9781119473206.ch3

Danyushevsky, L.V., Plechov, P. (2011) Petrolog3: Integrated software for modeling crystallization processes. *Geochemistry, Geophysics, Geosystems* 12, Q07021. https://doi.org/10.1029/2011GC003516

Ford, C.E., Russell, D.G., Craven, J.A., Fisk, M.R. (1983) Olivine-Liquid Equilibria: Temperature, Pressure and Composition Dependence of the Crystal/Liquid Cation Partition Coefficients for Mg, Fe^{2+}, Ca and Mn. *Journal of Petrology* 24, 256–266. https://doi.org/10.1093/petrology/24.3.256

Frost, B.R. (1991) Introduction to oxygen fugacity and its petrologic importance. *Reviews in Mineralogy and Geochemistry* 25, 1–9. https://doi.org/10.1515/9781501508684-004

Hu, F., Jiang, H., Wan, B., Ducea, M.N., Gao, L., Wu, F.-Y. (2024) Latitude-dependent oxygen fugacity in arc magmas. *Nature Communications* 15, 6050. https://doi.org/10.1038/s41467-024-50337-6

Kelley, K.A., Cottrell, E. (2009) Water and the Oxidation State of Subduction Zone Magmas. *Science* 325, 605–607. https://doi.org/10.1126/science.1174156

Kelley, K.A., Cottrell, E. (2012) The influence of magmatic differentiation on the oxidation state of Fe in a basaltic arc magma. *Earth and Planetary Science Letters* 329–330, 109–121. https://doi.org/10.1016/j.epsl.2012.02.010

Kress, V.C., Carmichael, I.S.E. (1991) The compressibility of silicate liquids containing Fe_2O_3 and the effect of composition, temperature, oxygen fugacity and pressure on their redox states. *Contributions to Mineralogy and Petrology* 108, 82–92. https://doi.org/10.1007/BF00307328

Mathez, E.A. (1976) Sulfur solubility and magmatic sulfides in submarine basalt glass. *Journal of Geophysical Research: Solid Earth and Planets* 81, 4269–4276. https://doi.org/10.1029/JB081i023p04269

Moussallam, Y., Oppenheimer, C., Scaillet, B., Gaillard, F., Kyle, P., Peters, N., Hartley, M., Berlo, K., Donovan, A. (2014) Tracking the changing oxidation state of Erebus magmas, from mantle to surface, driven by magma ascent and degassing. *Earth and Planetary Science Letters* 393, 200–209. https://doi.org/10.1016/j.epsl.2014.02.055

Moussallam, Y., Edmonds, M., Scaillet, B., Peters, N., Gennaro, E., Sides, I., Oppenheimer, C. (2016) The impact of degassing on the oxidation state of basaltic magmas: A case study of Kīlauea volcano. *Earth and Planetary Science Letters* 450, 317–325. https://doi.org/10.1016/j.epsl.2016.06.031

Moussallam, Y., Longpré, M.-A., McCammon, C., Gomez-Ulla, A., Rose-Koga, E.F., Scaillet, B., Peters, N., Gennaro, E., Paris, R., Oppenheimer, C. (2019) Mantle plumes are oxidised. *Earth and Planetary Science Letters* 527, 115798. https://doi.org/10.1016/j.epsl.2019.115798

Moussallam, Y., Georgeais, G., Rose-Koga, E.F., Koga, K.T., Hartley, M.E., Scaillet, B., Oppenheimer, C., Peters, N. (2023) CO_2-Undersaturated Melt Inclusions From the South West Indian Ridge Record Surprisingly Uniform Redox Conditions. *Geochemistry, Geophysics, Geosystems* 24, e2023GC011235. https://doi.org/10.1029/2023GC011235

Moussallam, Y., Oppenheimer, C., Scaillet, B. (2024) A novel approach to volcano surveillance using gas geochemistry. *Comptes Rendus. Géoscience* 356, 71–84. https://doi.org/10.5802/crgeos.158

Muth, M.J., Wallace, P.J. (2021) Slab-derived sulfate generates oxidized basaltic magmas in the southern Cascade arc (California, USA). *Geology* 49, 1177–1181. https://doi.org/10.1130/G48759.1

Osborn, E.F. (1959) Role of Oxygen Pressure in the Crystallization and Differentiation of Basaltic Magma. *American Journal of Science* 257, 609–647. https://doi.org/10.2475/ajs.257.9.609

Parkinson, I.J., Arculus, R.J. (1999) The redox state of subduction zones: insights from arc-peridotites. *Chemical Geology* 160, 409–423. https://doi.org/10.1016/S0009-2541(99)00110-2

Shorttle, O., Moussallam, Y., Hartley, M.E., Maclennan, J., Edmonds, M., Murton, B.J. (2015) Fe-XANES analyses of Reykjanes Ridge basalts: Implications for oceanic crust's role in the solid Earth oxygen cycle. *Earth and Planetary Science Letters* 427, 272–285. https://doi.org/10.1016/j.epsl.2015.07.017

Sun, C., Lee, C.-T.A. (2022) Redox evolution of crystallizing magmas with C-H-O-S volatiles and its implications for atmospheric oxygenation. *Geochimica et Cosmochimica Acta* 338, 302–321. https://doi.org/10.1016/j.gca.2022.09.044

Zhang, H.L., Cottrell, E., Solheid, P.A., Kelley, K.A., Hirschmann, M.M. (2018) Determination of $Fe^{3+}/\Sigma Fe$ of XANES basaltic glass standards by Mössbauer spectroscopy and its application to the oxidation state of iron in MORB. *Chemical Geology* 479, 166–175. https://doi.org/10.1016/j.chemgeo.2018.01.006

Zhao, S.-Y., Yang, A.Y., Langmuir, C.H., Zhao, T.-P. (2022) Oxidized primary arc magmas: Constraints from Cu/Zr systematics in global arc volcanics. *Science Advances* 8, eabk0718. https://doi.org/10.1126/sciadv.abk0718